ACS SENSORS

pubs.acs.org/acssensors
Article

Optogenetic Microwell Array Screening System: A High-Throughput Engineering Platform for Genetically Encoded Fluorescent Indicators

Michael Rappleye, Sarah J. Wait, Justin Daho Lee, Jamison C. Siebart, Lily Torp, Netta Smith, Jeanot Muster, Kenneth A. Matreyek, Douglas M. Fowler, and Andre Berndt*

Cite This: *ACS Sens.* 2023, 8, 4233–4244
Read Online

ABSTRACT: Genetically encoded fluorescent indicators (GEFIs) are protein-based optogenetic tools that change their fluorescence intensity when binding specific ligands in cells and tissues. GEFI encoding DNA can be expressed in cell subtypes while monitoring cellular physiological responses. However, engineering GEFIs with physiological sensitivity and pharmacological specificity often requires iterative optimization through trial-and-error mutagenesis while assessing their biophysical function *in vitro* one by one. Here, the vast mutational landscape of proteins constitutes a significant obstacle that slows GEFI development, particularly for sensors that rely on mammalian host systems for testing. To overcome these obstacles, we developed a multiplexed high-throughput engineering platform called the optogenetic microwell array screening system (Opto-MASS) that functionally tests thousands of GEFI variants in parallel in mammalian cells. Opto-MASS represents the next step for engineering optogenetic tools as it can screen large variant libraries orders of magnitude faster than current methods. We showcase this system by testing over 13,000 dopamine and 21,000 opioid sensor variants. We generated a new dopamine sensor, dMASS[1], with a >6-fold signal increase to 100 nM dopamine exposure compared to its parent construct. Our new opioid sensor, μMASS[1], has a ∼4.6-fold signal increase over its parent scaffold's response to 500 nM DAMGO. Thus, Opto-MASS can rapidly engineer new sensors while significantly shortening the optimization time for new sensors with distinct biophysical properties.

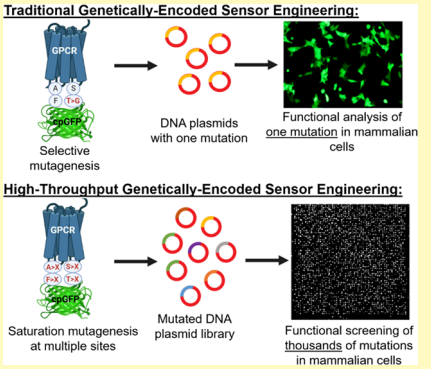

KEYWORDS: *fluorescent biosensor, GPCR, dopamine, opioids, high throughput screening, protein engineering*

Genetically encoded fluorescent indicators (GEFIs) are protein-based sensors that detect specific ligands and change their fluorescence intensity ($\Delta F/F_o$) through allosteric interactions with a fused fluorophore.[1−3] They enable the dynamic imaging of ions and intra- and extracellular compounds and provide a comprehensive view of their dynamics in cells and tissues. Recently, a new family of GEFI was engineered by grafting a circularly permuted fluorophore (cpGFP) into the third intracellular loop of dopamine G-protein coupled receptors (GPCRs) (Figure 1A).[4,5] Moreover, the cpGFP insertion has worked with a range of GPCRs.[6] Thus, GPCR-based indicators now include sensors for dopamine, acetylcholine, serotonin, norepinephrine, and orexin.[7−10] These GEFIs can be expressed in specific neuron subtypes, detect neurotransmitter or neuromodulator release in freely behaving animals, and establish time-locked causal correlations to motivated behaviors. Nevertheless, current GEFI scaffolds typically require further optimization of biophysical properties, such as dynamic range and ligand binding affinity, to enhance their function *in vivo*. Optimizing new indicators usually requires laborious testing of mutated variants by iterative trial-and-error approaches one-by-one. Accordingly, the several hundred variants screened for recently developed sensors represent only a small fraction of the mutational landscape of the targeted residues, often less than 1%. Therefore, the current methods of sensor engineering are far from optimal. Another significant difficulty of GPCR sensor engineering is that results from high-throughput systems using bacteria, yeast, or isolated proteins often do not translate well to mammalian cells.[11,12] On the other hand, mammalian host cells such as HEK293 cultures have not yet reached the necessary high-throughput capabilities for more efficient sensor testing. Individual plasmids encoding the mutated sensor genes must be transfected into cells seeded in multiwell plates (24–384 wells) and then tested one-by-one, thus severely limiting throughput. In our experience, these approaches limit testing

Received: July 31, 2023
Revised: October 3, 2023
Accepted: October 24, 2023
Published: November 13, 2023

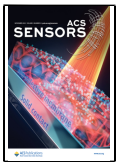

https://doi.org/10.1021/acssensors.3c01573
ACS Sens. 2023, 8, 4233–4244

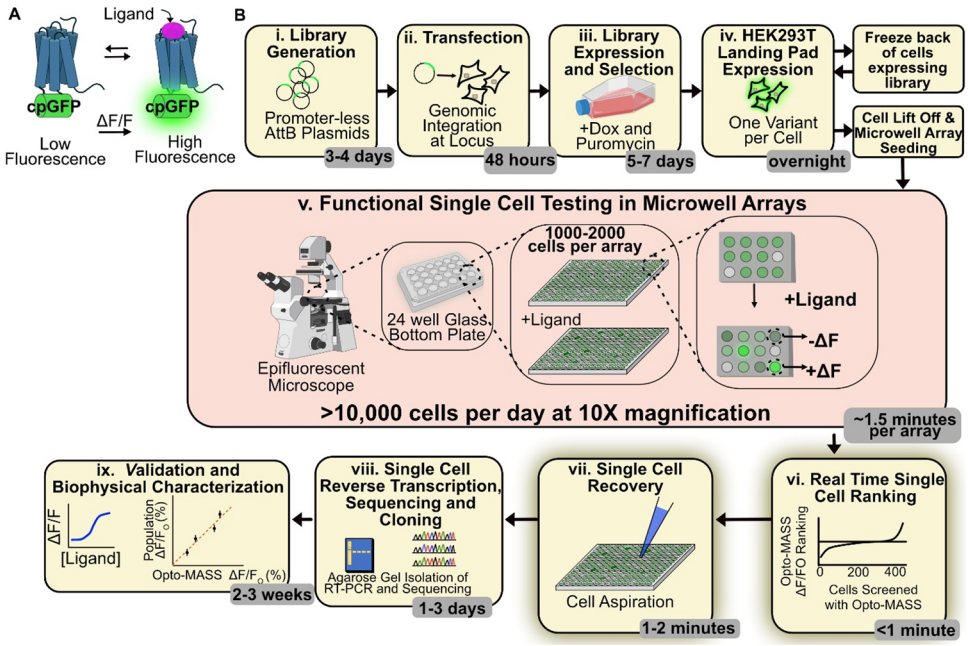

Figure 1. Overview of the Optogenetic Microwell Array Screening System (Opto-MASS) (A) Schematic of sensor topology and basic function. GPCR sensing domains bind the ligand of interest. The ligand binding induces conformational changes, which allosterically increases the cpGFP fluorescence emission. (B) Opto-MASS combines microwell array screening and mammalian genetic expression to rapidly screen thousands of cells/variants of sensors on a platform that can complete sensor engineering in less than one month. First, a randomized mutational library of the sensor is constructed in landing pad-compatible plasmids. The library is recombined into a single locus in the HEK293T "landing pad" cell genome. After doxycycline induction and puromycin selection for 5−7 days, the library can be frozen for later screening or seeded onto microwell arrays. The Opto-MASS microwell arrays are screened on an inverted fluorescent microscope, and sensors are ranked in parallel in each field of view. After identifying the highest-performing cells, a glass micropipette is used to aspirate them physically. Next, we used RT-PCR to identify the underlying sensor gene. The recovered gene is then transfected into HEK293 cell cultures to characterize the sensor's biophysical phenotype in detail on a population level.[38]

to several hundred variants in 6 to 12 months. Moreover, there are over 800 mammalian GPCRs with unique pharmacological profiles and physiological roles, presenting a monumental task for protein engineers to construct a sensor for each GPCR optimized by mutational trial-and-error.[13]

Several recent studies aimed to establish more efficient, high-throughput testing for genetically encoded calcium and voltage indicators in mammalian cells[14,15] (Table 1). Both of these approaches utilized electrical field stimulation to test the function of the biosensors; however, this limited the throughput of functionally tested variants to either tens or low hundreds in library screens. Another strategy used *in vitro* coupled transcription/translation to screen soluble lactate sensors in gel-shell beads (GSB), dubbed BeadScan.[16] The GSB technique enabled multiparameter screening of approximately 2,000 soluble biosensor variants. However, this approach precludes membrane-bound GPCR-based sensors due to the lack of cell membranes in the screening system. Another cell-based high-throughput screening method, Faculae, utilizes FACS sorting to pool advantageous mutations in fluorescent sensors. The method relies on oversampling and consequently, the effective library sizes were relatively small.[17] CRISPR/Cas9 has been used to engineer the fluorescent reporter mCRISPRed by mutating proteins directly in mammalian host cells.[18] The functional readout was conducted by FACS sorting, which can only measure baseline fluorescence and does not provide dynamic changes in fluorescent proteins. Our goal for this work was to develop a platform that enables dynamic testing of thousands of sensor variants in a mammalian host system within minutes to hours. To that end, we developed an optogenetic microwell array screening system (Opto-MASS). Opto-MASS isolates HEK293T cells in individual microwells (typically 1000−2000 cells), where each cell expresses a single mutated GEFI variant. Isolating single cells, expressing a single variant in each microwell, generates an array of small "reactors" where we can interrogate and multiplex the biophysical characteristics of many GEFIs simultaneously. Specific ligands stimulate all variants at the same time, while fluorescence signals are measured simultaneously. Cells expressing a desirable phenotype (e.g., large signal amplitudes) are identified in real-time and physically recovered. The gene encoding the sensor is then retrieved, sequenced, and characterized in a population of mammalian cells for cross-validation. In summary, Opto-MASS provides functional screening of thousands of biosensor variants, exceeding the throughput of most common approaches.

EXPERIMENTAL METHODS

Microwell Array Fabrication. The master mold (negative) of the microwell arrays was fabricated using ICP4-SPTS-DSi using deep reactive ion etching (DRIE) for etching silicon wafers. To prepare the wafer for DRIE, we spun AZ1512 photoresist (MicroChemicals) onto 100 mm silicon wafers (University Wafer) with a two-step process. First, wafers were spun at 500 rpm for 5 s to spread the photoresist and a final 30 s spin step at 2500 rpm. After incubation at 100 °C for 60 s on a hot plate, the wafer was exposed to a chrome-on borosilicate glass mask and developed with AZ340 developer (MicroChemicals).

Polydimethylsiloxane (PDMS) (Sylgard 184, Corning) was used to construct the microwell arrays. The elastomer and the curing agent were thoroughly mixed at a ratio of 10:1 (w/w), poured onto the

https://doi.org/10.1021/acssensors.3c01573
ACS Sens. 2023, 8, 4233−4244

Table 1. Summary of the High-Throughput Techniques Used to Engineer Genetically Encoded Fluorescent Sensors

platform title	genetically encoded indicator type	host system	# of sensor variants functionally tested	stimulation modality
Opto-MASS	GPCR-based indicators	HEK293T TetBxb1BFP	>10,000 per sensor type	Bath ligand application
A neuron-based screening platform for optimizing genetically encoded calcium indicators 14	calcium indicators	primary rat hippocampal neurons	447 in 2 662 in 37	electrode stimulation to induce neuronal Ca^{2+} transients upon action potential firing
A robotic multidimensional directed evolution approach applied to fluorescent voltage reporters 15	voltage Indicators	HEK293T cells	round one: 48, round two screening: 216	electrodes to induce field potential changes
A high-throughput multiparameter screen for accelerated development and optimization of soluble genetically encoded fluorescent biosensors 16	lactate sensors	Gel-shell beads - total *in vitro* transcription/translation system	2196	ligand dependent fluorescence lifetime (2P-FLIM), pH (ligand addition), microfluidic cell retrieval
Functional imaging-guided cell selection for evolving genetically encoded fluorescent indicators 17	calcium indicators	HEK293T cells landing pad	400 and 8000	bath ligand addition

silicon wafer, and placed in a desiccator to remove air bubbles. After the air bubbles were removed, the wafer was moved to a 55−75 °C incubator to cure for several hours.

After curing, PDMS was removed using razor blades and forceps. The PDMS was plasma treated for 60 s and then firmly pressed onto a dried bovine serum albumin (BSA) layer to nanostamp a layer of BSA onto the surface (FischerSci Cat# BP1600). The dried BSA layer was made by incubating a 2% w/v solution of BSA in PBS in a Petri dish for approximately 30 min. After, the dish was rinsed 3× with PBS and left to dry. After the plasma-charged PDMS was pressed into the BSA, debris was removed from the back of the PDMS using tape. The PDMS microwell arrays were cut out using a scalpel and placed upright into a glass-bottom 24-well dish.

Building Genetic Libraries for Screening on the Platform. Gibson Assembly was used to build the genetic libraries of sensors. The insert and backbone were PCR amplified using Q5 polymerase (New England Biolabs (NEB) M0515) and degenerate codons (IDT) were introduced with primers during PCR amplification of the cpGFP insert. To subclone the cpGFP moiety with two flanking mutational regions, we used primers to amplify the cpGFP domain out of a mammalian expression plasmid containing GCaMP6f. One μL of DpnI was used to digest the PCR templates. PCR products were isolated from a 1% agarose gel stained with SyberSafe (Invitrogen cat. #S33102) and the New England Biolabs (NEB) Monarch DNA Gel Extraction Kit (cat. # T1020L). After gel isolation, the insert and backbone were assembled using NEB HiFi DNA assembly (NEB cat. #: E2621). A total of 0.2 pmol of DNA was used in the Gibson Assembly, with a 6:1 molar ratio of insert (cpGFP moiety) to vector and incubated at 50 °C for 60 min.

The assembly was cleaned by using an NEB PCR cleanup kit and double-eluted from the column with 10 μL of prewarmed water. We then transformed 33 μL of electrocompetent cells (NEB cat no. C3020K) (2000 V, τ = 5 ms) in ice-cold cuvettes (1 mm gap) with 2 μL of the elution. Immediately after the cells were pulsed, 967 μL of prewarmed SOC media was added to the cuvettes. After 1 h of recovery at 37 °C and 240 rpm in a 15 mL recovery tube, a dilution of the recovery media was plated on an agar plate and grown overnight to estimate library size. The remaining recovery media was added to 125 mL of Luria Broth (LB) with ampicillin and grown overnight at 37 °C and 240 rpm. The 15 mL recovery tube was rinsed several times with fresh LB media to ensure that all transformants were added to the larger overnight culture.

After overnight growth, the agar plate was counted to estimate the total transformants, and colonies were randomly selected for library sampling. Library plasmids were isolated from liquid culture using the Machery−Nagel NucleoBond Xtra Midi EF kit (ref # 740420.50). The resulting plasmid prep was used to generate stably integrated cell lines with the landing pad cell line. The dopamine sensor and MOR sensor libraries used templates from ref 4. During library screening, the MOR sensor template had an IgK sequence attached to the N terminus and a TSER signal attached to the C-terminus. The IgK sequence was removed from the μMASS[1] sensor during *in vitro* biophysical characterization.

Library Transfection into Landing Pad Cells. After validation that the library was correctly assembled in transformed *E. coli* through Sanger Sequencing of selected colonies, HEK293T landing pad cells were stably recombined with our library using a double transfection protocol. Landing pad cells were maintained in standard growth media supplemented with 1−2 μg/mL doxycycline. On the day of transfection, the cells were gently lifted off the growth substrate using 0.05% Trypsin/EDTA (Invitrogen cat. # 25300120). Liftoff was stopped by adding growth media. Approximately 250,000 cells per well were seeded into each well of 6-well dishes, and the final culture volume per well was raised to 2 mL. The DNA transfection reagents were prepared by incubating 3 μg of plasmid DNA encoding the Bxb1 recombinase and 6 μL of Fugene6 reagent (Promega cat. # E2693) in 300 μL of Opti-MEM for 15 min and then added to the cell suspension. After 24 h of incubation, cells were lifted off the growth substrate and centrifuged at 500 RCF for 5 min. After seeding at 250,000 cells/well in a 6-well dish, the cells were transfected with

https://doi.org/10.1021/acssensors.3c01573
ACS Sens. 2023, 8, 4233−4244

library plasmids using the same protocol used for Bxb1 recombinase transfection. For each round of library screening, five wells of the six-well plate were transfected with the genetic library and combined after puromycin selection for screening. Note, while still in the genome of the HEK293T cells, the BFP expression is ceased as the poly-A tail and stop codon of the gene of interest stop its expression. BFP is slowly degraded by the cells.

Cell Seeding. The nanostamped PDMS microwell arrays were then briefly plasma-treated to charge the inner wells. Quickly after plasma treatment, standard growth media was added to the wells, and they were placed in a desiccator to remove bubbles in the microwells. The plates were briefly returned to the tissue culture incubator to raise the temperature of the media and balance the pH. Next, the landing pad cells were lifted from the growth substrate with 0.05% Trypsin/EDTA and triturated to achieve a single-cell suspension. Once a single cell suspension was achieved, the cells were counted, and then 40K cells were seeded at a concentration of 0.5×10^6 onto the arrays. Cells were slowly pipetted above the array with a micropipette. The cells were returned to the incubator for 10 min. After 10 min, the 24-well plates were then placed in a centrifuge and spun down at 100 RCF for 5 min. The arrays were then rinsed with growth media several times to remove cells not seeded in microwells and cell debris. The final rinse is with DMEM/10% FCS supplemented with doxycycline at the concentration used during selection and half-selection of puromycin concentration. The cells were then returned to the incubator overnight for screening the following morning.

Library Screening and Cell Selection. On the morning of cell selection experiments, the arrays were washed twice with standard growth media and once with imaging Tyrode's supplemented with GlutaMax (Gibco ref: 35050−1), sodium pyruvate (GIBCO ref: 11360−070), and MEM Nonessential Amino Acids (Gibco ref: 11140−050). A MetaMorph software Journal was used to control the microscope during imaging. In brief, the control fluorophore was imaged before and after stimulation (mCherry, 578/21 nm excitation, 641/75 nm emission); for stimulation imaging, arrays were imaged under GFP excitation/emission (474/27 nm excitation, 520/35 nm emission) continually for 1 min. Ligands were added by an automatic pump or hand to the bath. The control fluorophore was imaged and a bright-field image. The images were then analyzed by using MetaMorph.

Arrays were imaged with an sCMOS camera (Photometrics Prime95B) on an epifluorescent microscope (Leica DMI8) using a 10× objective (Leica HC PL FLUOTAR L 10x/0.32 NA). A Lumencor Light Engine LED, and Semrock Filters were used for fluorescence imaging. The Tyrode (125 mM NaCl, 2 mM KCl, 2 mM $CaCl_2$, 2 mM $MgCl_2$ 30 mM Glucose, and 25 mM HEPES) used for imaging was supplemented with GlutaMax (Gibco ref: 35050−1), sodium pyruvate (GIBCO ref: 11360−070), and MEM non-essential amino acids (Gibco ref: 11140−050) and pH balanced to 7.3−7.4. Ligands were prepared in a Tyrode's solution.

To briefly summarize the image analysis in MetaMorph, masks to identify regions of interest (ROIs) were generated by using before and after control fluorophore images. A Logical AND of pixels above a threshold from the pre- and poststimulation was used to identify ROIs and remove any ROIs that shifted out of microwells during stimulation. ROIs were defined with this mask. ROIs were transferred to the stimulation stack. The stimulation stack was split into pre- and postligand addition. The average fluorescence intensity of the pre- and postligand addition stacks was calculated. The average fluorescence intensity images were divided and multiplied by 1000, generating the array rank ratio image. The ROIs were copied to the array rank ratio image, and the mean fluorescence intensity for each ROI was calculated and used to determine an ROI rank. The top 10 responding ROIs were transferred to a copy of the stimulation stack and the Live Field of view. The user can verify the authenticity of the ROIs prior to physical recovery of the cells. Glass micropipets used to recover the cells. In brief, the ROI highlighting the cell of interest is transferred to the field of view. Using a micromanipulator, patch glass micropipettes with a slight positive pressure applied are navigated to the ROI containing the cell of interest. Positive pressure is released, and slight negative pressure is applied with a syringe as the micropipette approaches the desired cell. After the cell and glass micropipet seal, the cell and tip are raised out of the bath and placed into a PCR tube where positive pressure is applied and the tip added to the tube. A new tip is used for the next cell. The micropipets were then transferred to 200 μL PCR tubes with 5 μL of a TE/DTT buffer and immediately placed on dry ice for the remainder of the screening session.

After the screening session was over, the samples were processed to convert sensor mRNA into cDNA using an adapted protocol of the ThermoFischer SuperScript IV reverse transcriptase (SSIV RT) protocol. Two μL of the cDNA product was then amplified in a 25 μL reaction mixture using Q5 polymerase. After DNA isolation on a 1% agarose gel and cleanup, the PCR product was Sanger sequenced to check for contamination and cloned into a pCMV backbone using Gibson assembly to validate the gene's performance. The plasmids were transfected into HEK293 WT cultures in plastic 24-well dishes to validate the performance of the gene.

Reverse Transcriptase Reaction. Single-cell recovery tubes were prepared by diluting 5 μL of 0.1 M DTT into 200 μL of TE buffer; 5 μL of the TE/DTT solution was added to each PCR tube. After a single cell was deposited into the tube, the tubes were incubated on dry ice for the remainder of the library screening session. After library screening, the tubes were removed from the dry ice and placed on wet ice. Each tube was processed with reagents from the SuperScript IV First-Strand synthesis kit (Invitrogen cat. # 18091050). To each tube, 0.5 μL of 0.1 M DTT and 0.5 μL of RNase inhibitor were added. The samples were then placed on dry ice for 5 min and then moved back to wet ice. Next, 0.5 μL of the following was added to each tube, DI H_20, a 10 mM dNTP mix, and 2 μM primer.

Next, the primers were annealed to the mRNA by incubating the samples at 95 °C for 30 s, 4 °C for 1 min, and 65 °C for 5 min. The samples were then returned to the wet ice. Next, 2 μL of SSIV RT 5× Master Mix was added to each sample. The samples were pipetted up and down thoroughly. Finally, 0.5 μL of the SSIV RT Enzyme was added to each tube, and the samples were thoroughly pipetted up and down. To perform the reverse transcriptase reaction, the samples were incubated at 53 °C for 10 min and then at 80 °C for 10 min. Next, 0.5 μL of RNaseH was added to each tube, and the samples were incubated for 20 min at 37 °C to remove any mRNA from the cDNA. Samples were stored at −20 °C before PCR amplification of cDNA with Q5 (New England Biolabs) or SuperFiII (ThermoFischer) using recombination-specific primers.

Transfection and Imaging for *In Vitro* Assays. HEK293 cells were cultured on tissue culture-treated plastic at 37 °C with a 5% CO_2 atm. One day prior to transfection, cells were lifted off the growth substrate with 0.05% Trypsin/EDTA. The cells were then seeded into 24 well tissue culture plates. Cells were grown to 70−80% confluency and then transfected. During transfection, the growth medium was replaced with fresh 250 μL of media. The DNA transfection reagents were prepared using the standard protocol. In brief, per well of transfection, 25 μL of Opti-MEM, 1 μg of DNA, and 1.5 μL of P3000 were mixed. After 5 min of equilibration, the Opti-MEM/DNA/P3000 mix was added to a tube containing 25 μL of Opti-MEM and 1.5 μL of Lipofectamine. The DNA/P3000/Lipofectamine mix was incubated for approximately 15 min at room temperature before adding it to the wells. After incubation for 3−4 h, the transfection medium was removed, and fresh medium was added. Reactions were scaled for different well sizes according to the manufacturer's directions.

Cells were imaged with an sCMOS camera (Photometrics Prime95B) on an epifluorescent microscope (Leica DMI8) using a 20× objective (Leica HCX PL FLUOTAR L 20x/0.40 NA CORR) 48 h after transfection. A Lumencor Light Engine LED and Semrock Filters were used for fluorescence imaging.

Before imaging, cells were rinsed once with triple-supplemented Tyrode's solution, as described above. Bath additions of ligands were made by hand for validation experiments, and the volume added was

https://doi.org/10.1021/acssensors.3c01573
ACS Sens. 2023, 8, 4233−4244

always equivalent to the preaddition bath volume. Ligands were prepared in a Tyrode's solution.

For confocal images of fluorescence responses, HEK293 cells were plated onto poly L-lysine (Cultrex 3438−100−01) coated glass bottom plates and imaged in Tyrode's solution with a Nikon A1R microscope with a 40× oil objective (CFI Plan Fluor NA 1.30) at room temperature (≈23 °C). A 488 nm laser was used for GFP and sensor imaging, and a 561 nm laser was used for red fluorophore imaging. Ligands were hand pipetted into the bath.

Fluorescence change graphs were generated by taking the average intensity projection of five frames before ligand addition and five frames after ligand addition using the FIJI image analysis software (NIH). The resulting images were then divided in MATLAB (2019a) to determine a pixel-by-pixel fluorescence change, and a color scale was overlaid.

Internalization Assay. Twelve mm glass coverslips were coated with poly L-lysine. After incubation in poly L-lysine for approximately one-two h at room temperature or overnight at 4 °C. After incubation, the coverslips were rinsed three times with 1× PBS. HEK293 cells were seeded onto the coverslips and grown to 70−80% confluency. The HEK293 cells were transfected using the above Lipofectamine 3000 reagents and protocol with an increased total amount of DNA (1500 ng per well and a 1:1 molar split between the control fluorophore plasmids and sensor expression plasmids. The first contained the pCMV mRuby-CaaX, and the other contained a pCMV rMOR eGFP or the pCMV μMASS[1] plasmid.

Forty-eight hours after transfection, the coverslips were imaged on an epifluorescence microscope with a 40× oil objective at 37 °C in prewarmed, triple supplemented Tyrode's solution (Tyrode's described as above). Cells were imaged for 1 h, during which they were sampled 60 times. A mCherry image and an eGFP image were taken at each time point. Images were analyzed in FIJI to collect intensity profiles, analyzed in Excel, and plotted in GraphPad Prism 8.

Affinity Curves. HEK293 cells were transfected with Lipofectamine 3000 reagents for the dopamine affinity curves. In brief, HEK293 cells were seeded onto poly-L-lysine coated 96-well glass-bottom plates, expanded to 70−80% confluency, and transfected. After transfection, the cells were incubated for 24−48 h before imaging.

Prior to imaging, cells were rinsed and imaged in 50 μL of supplemented Tyrode's solution. During imaging, 150 μL of the ligand and Tyrode's solution were added to the bath during imaging. Cells were imaged with a 63× air objective.

For the peptide affinity curves, landing pad cells expressing the μMASS[1] sensor were used. Cells were seeded at 25,000 cells per well in a 96 well dish and imaged the next day after overnight growth in 8 μg/mL doxycycline. A 63× air objective was used to image the cells continuously for 60 s. 150 μL of peptide solution was hand pipetted into a bath of 50 μL bath.

Cells were analyzed using FIJI (NIH). Five to six cells from each well were hand circled from background-subtracted image stacks (Rolling ball, 100 pixels). The average fluorescence intensity was measured for each cell and exported to Excel for analysis. Analyzed data were imported into GraphPad Prism 8 to calculate K_d values using the nonlinear fit function to normalize responses and logarithm concentrations. Single site binding was assumed. Least squares fit was used.

Dopamine Sensor Affinity Curves. Twenty-thousand HEK293 cells were seeded onto poly-L-lysine coated 96-well glass-bottom plates. Twenty-four hours after seeding, cells were transfected with 400 ng of pCMV plasmids using Lipofectamine 3000 reagents. In brief, growth media was removed, and 50 μL of media was added to each well. Lipofectamine 3000 reagents were prepared according to the same protocol as described above but scaled down for 96-wells. For 96 well plates, 5 μL of Opti-MEM, 400 ng of DNA, and 0.4 μL of P3000 were added to tube A, per well. A total of 0.4 μL of Lipofectamine 3000 was diluted in 5 μL of Opti-MEM per well in tube B. The plasmids expressed a GPCR sensor and a membrane bound control fluorophore, mRuby3_CaaX, separated by a self-cleaving P2A peptide. Twenty-four hours after addition of the DNA/Opti-MEM/lipofectamine mixture to the wells, the medium was removed and fresh growth medium was added.

Forty-eight hours after transfection, media was removed and cells were rinsed with imaging Tyrode's solution. Well volume was set to 150 μL of Tyrode's solution. Plates were moved to the Odyssey M imager and imaged under green and red fluorophore excitation. 50 μL of drug solution was added to each well, and the plate was imaged again. In-cell, 96 well plate imaging at a 2.45 mm offset was used to image both red/green fluorophore excitation and emission. Images were analyzed in FIJI and green fluorescence values were normalized to red fluorescence values for both the apo and ligand states. Drug dependent fluorescence changes (background) were subtracted by averaging the fluorescence response to wells containing HEK293 cells with no sensor transfection, and 100 μM ligand was added. GraphPad Prism 9 was used to generate the affinity curves. K_d values were calculated using a logarithm scale for concentrations and normalizing the maximum sensor response to 100% and the minimum to 0%. Single site binding was assumed.

A 488 nm laser was used at 5% power. Heatmaps were generated by using a custom MATLAB script.

Calculation of $\Delta F/F_o$. The change in fluorescence was measured by hand circling regions of interest (ROIs) around background-subtracted images in FIJI. The ROIs were measured for mean gray value over time. The measurements were imported into Excel, where eq 1 was used to calculate the change in fluorescence:

$$\Delta F/F_o(\%) = \frac{(F_i - F_{baseline})}{F_{baseline}} \times 100 \quad (1)$$

where F_i is the ROI mean fluorescence for a frame and $F_{baseline}$ is the average fluorescence for the first five or six frames after imaging began. When peak fluorescence is shown, the maximum fluorescence is identified in a time course, and five frames surrounding maximum fluorescence are averaged to account for noise in the fluorescence measurement.

Molecular Cloning. Unless explicitly stated, DNA constructs were cloned with either Q5 polymerase, Platinum SuperFi II, site-directed mutagenesis, Gibson assembly, *in vitro assembly*, or standard restriction enzyme cloning. PCR products were verified on 1% agarose gels stained with SyberSafe and cleaned with NEB Monarch PCR Clean-Up kits. The pCAG NLS HA bxb1 plasmid was gifted from the Fowler lab (Addgene no. 51271); the AttB puromycin plasmid used to generate libraries was gifted from the Fowler lab; the pCMV dLight1.1 plasmid was sourced from Addgene (#111053), and rat MOR plasmid was a gift from the Bruchas Lab.

RESULTS AND DISCUSSION

Opto-MASS required complex interdisciplinary integration of microfabrication processes, genome science, molecular biology, and image processing (Figure 1B). It was specifically developed to integrate four distinct steps necessary for the efficient high-throughput testing of mutational GEFI libraries in mammalian host cells.

To generate extensive and unbiased DNA libraries, we conducted PCRs with randomized primers during library construction (Figure 1B(i). The PCRs introduce codons for all 20 amino acids at selected residues in the GEFI encoding genes. The resulting protein library sizes depend on the number of targeted residues, e.g., 1 residue = 20 variants, 2 residues = 400 variants, 3 residues = 8000 variants, etc.

DNA library expression requires an efficient and cost-effective technique for mammalian host cells, enabling easy linkage of GEFI phenotype to genotype. We incorporated the "landing pad" HEK293T TetBxb1BFP cells as our host system to address a critical problem and directly link genotype to phenotype by expressing a

https://doi.org/10.1021/acssensors.3c01573
ACS Sens. 2023, 8, 4233−4244

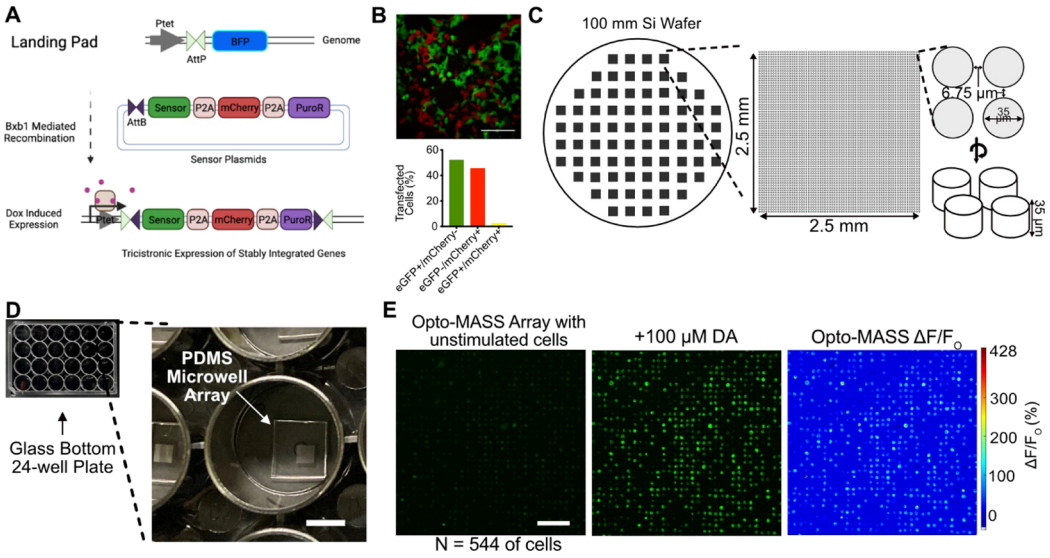

Figure 2. Design and engineering of an optogenetic microwell array screening system. (A) Schematic of the genomic landing pad in the HEK293T landing pad cells (HEK 293T TetBxb1BFP) pre- and postintegration of the sensor encoding plasmid by Bxb1 recombinase.[38] (B) Demonstration of the landing pad system. Representative false-color image of HEK293T TetBxb1BFP cells transfected with an equimolar mixture of plasmids containing either mCherry or eGFP (top panel, 100 μm scale bar). Summary data for the field of view for fluorophore expression (lower panel). The majority of cells express only one fluorophore. (C) Silicon master mold of the microwell arrays (left), dimensions of one array (middle), and individual microarrays (right). The Si wafer was etched using deep reactive ion etching. The individual 3600 wells are designed to hold only one HEK293T cell. (D) Polydimethylsiloxane (PDMS) microwell arrays are cut from the master mold after curing and BSA nanostamping and are placed "wells up" in the bottom of a 24-well glass bottom plate for cell seeding and subsequent screening. (E) Representative stimulation of an isogenic population of landing pad cells expressing dLight1.3b and stimulated at saturation with 100 μM dopamine on the Opto-MASS array. N = 544 cells.

single variant per cell (Figure 1B(ii–iv)).[19] They contain an engineered "landing pad" in the genome where a single plasmid is irreversibly recombined and expressed after transfection (Figure 2A). Our library plasmids encode three genes on a tricistronic cassette, the green fluorescent GPCR sensor, red-fluorescent mCherry (control for image analysis), and a puromycin resistance gene (selection of recombined cells), each separated by self-cleaving P2A sequences. Thus, while transfection reagents can introduce more than one library plasmid per cell, only one plasmid can recombine and express in the genomic landing pad. We demonstrated this system by transfecting an equimolar mixture of two plasmids encoding either only eGFP or mCherry (Figure 2B).

We physically separate host cells in customized polydimethylsiloxane (PDMS) microwell arrays, allowing fast and detailed analysis of fluorescent signals from each cell. (Figure 1B(v)). We fabricated a negative master mold from a silicon wafer using deep reactive ion etching (Figure 2C). We designed the arrays for optimal cell seeding density at a size of 2.5 × 2.5 mm and 35 μm well diameter, 6.75 μm spacing, and 35 μm well depth resulting in 3600 wells per array. The PDMS arrays are cast by standard soft lithography techniques and cut before being placed in 24-well plates (Figure 2D). We optimized cell seeding to maximize well occupancy while reducing the occurrence of multiple cells in a microwell. We found the optimal conditions for seeding at ~40,000 HEK293T cells at a concentration of 0.5 × 10^6 cells/mL per array. This results in single cell occupied wells at about 30–50% total occupancy, routinely providing up to 1800 observable cells at 5× or 300–600 cells at 10× magnification. Once seeded into microwells and activated by ligands, the fluorescence responses were automatically analyzed and ranked by signal amplitude ($\Delta F/F_0$) in real-time (Figures 2(vi) and 2E). Our automated real-time image analysis excluded cells that were moving in or out of the field of view during screening (Figure S1A–C).

The highest performing cells were physically aspirated by glass pipettes, and the sensor genes were retrieved using RT-PCR followed by sequencing of the resulting cDNA (Figure 1B(vii–viii)).

Opto-MASS Identifies Functionally Diverse Sensor Variants From DNA Libraries. For the validation of the Opto-Mass platform, we chose dopamine sensor dLight1.1 as a scaffold. Its robust responses make it suited for optimizing all aspects of the screening platform. Furthermore, the initial optimization strategy for dLight1.1 created diverse responses in sensor variants but left the vast majority of potential variants untested.[4,20] We targeted the same four residues directly flanking either side of the cpGFP insertion into the human D1 dopamine receptor (Figure 3A). These residues play a critical role in coupling fluorophore brightness to ligand-dependent conformational changes in the receptor domain. Still, in the previous study, only 585 out of the 160,000 possible protein variants were tested.[4] We built a library of randomized mutations with an even distribution of nucleic acids at the targeted sites (Figure 3B, > 200,000 *E. coli* transformants). By targeting four amino acids with NNK codons, our library size is 32^4 (~1 × 10^6) at the DNA level and 160,000 protein variants. After the library was stably expressed, the HEK293T cells were seeded onto microwell arrays and allowed to recover for 12–16 h. The cells were then stimulated and imaged under epifluorescence (474 nm excitation, 520 nm emission, 200 ms exposure) (Figure 3C). Note that the simultaneous increase in

https://doi.org/10.1021/acssensors.3c01573
ACS Sens. 2023, 8, 4233–4244

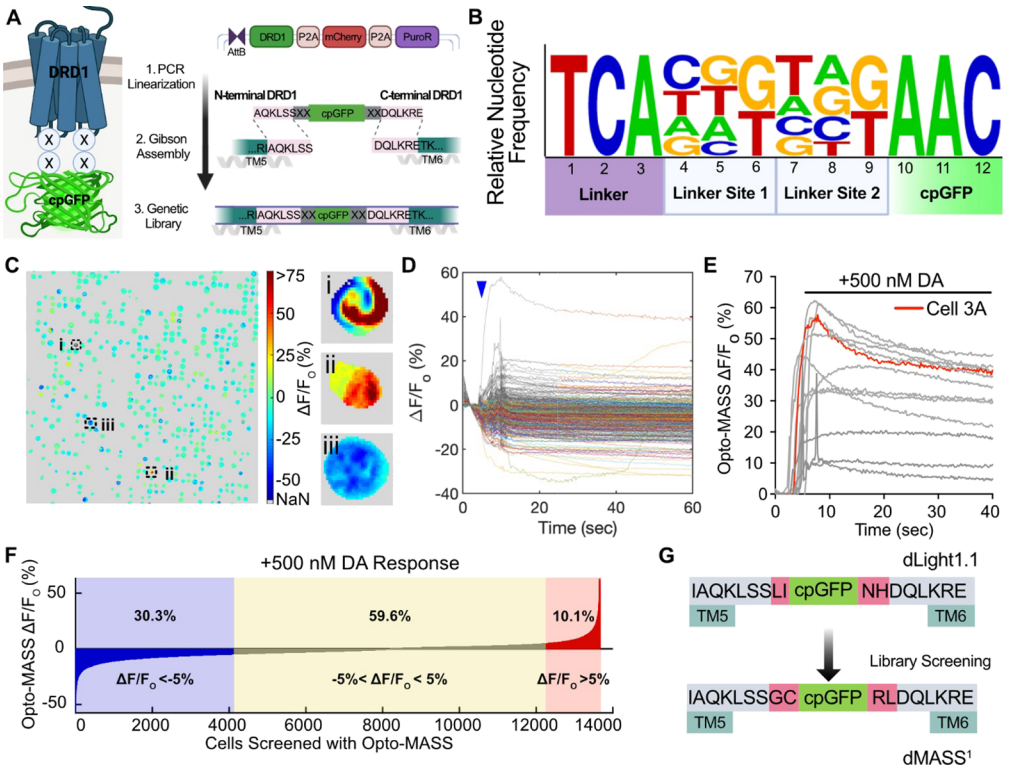

Figure 3. Mesoscale screening of linker library yields improved dopamine sensor. (A) Left: schematic of the residues targeted for generating a mutational dopamine sensor library from dLight1.1 (denoted by X). The four residues are located in the linker between the cpGFP and GPCR DRD1 domains and were targeted by site-saturated randomized mutagenesis. Right: schematic of the dopamine sensor library construction using a Gibson Assembly. DNA primers with four randomized codons (NNK) encoding four residues (X) in both peptide linkers within the dopamine sensor were used to construct the library. The targeted linker regions are located between the dopamine receptor DRD1 and cpGFP. The resulting inserts encode a peptide linker with six randomized bases on both sides (i.e., two residues on N and C terminal sides each). The final library plasmids also encode red fluorescent mCherry as control, which is located on the DNA backbone.[38] (B) Summary of 23 sampled sequencing results, from the c-terminal linker reveals near equal distribution of all possible nucleotides (NNK) at the targeted sites. (C) Heat map of pixel intensity changes in the ROI mask upon dopamine addition to one array with a dopamine sensor library expressing landing pad cells (439 cells). Note that areas outside the mask were assigned a gray value. Inset panels (i-iii) are areas of interest showing the platform can identify varying signal amplitudes from individual cells. (D) Individual time-resolved traces of green fluorescence dynamic extracted from the generated ROI mask shown in (C). Cells were stimulated with 500 nM dopamine. The blue arrow denotes the approximate time of the DA addition. Signals during the presence of motion artifacts due to DA addition were excluded. (E) Exemplary responses of selected cells from the entire screen over 24 arrays. A high-performing cell (red, 3A) was retrieved and named dMASS[1]. dMASS[1] was extensively validated in subsequent experiments in HEK293 cell populations. (F) Aggregate responses from one screening session of the dopamine sensor library stimulated with 500 nM DA. 13,656 cells were screened in 1 day. A total of 30.3% of the screened cells had a dopamine (DA) dependent decrease in fluorescence ($\Delta F/Fo < -5\%$) 59.6% had no change in fluorescence and 10.1% had an increase in fluorescence ($\Delta F/Fo > 5\%$). (G) dMASS1 mutations in both linker regions were identified by RT-PCR and Sanger sequencing postscreening and compared to dLight1.1. All targeted bases were mutated in dMASS[1] compared to dLight1.1.

fluorescent signals from the cells demonstrates that diffusion of the dopamine (500 nM) was immediate (Figure 3D). We ranked cells by ligand-dependent fluorescence change and aspirated the 13 highest ranking cells from all arrays using glass micropipettes (Figures 3E). Cells were placed into separate microcentrifuge tubes containing dithiothreitol (DTT) to prevent RNA degradation for subsequent sensor cDNA retrieval by single-cell RT-PCR.

In one of our first trials, we screened ~13,000 cells (Figure 3F) with 500 nM dopamine stimulation and ranked their individual response amplitudes. Importantly, we screened at nonsaturating ligand concentrations, aiming to identify a variant that has an optimal allosteric coupling between domains at low concentrations of dopamine. In contrast, previous studies screened under saturating DA concentrations and risked missing variants with strong allosteric coupling at low ligand concentrations. A total of 30.3% of cells decreased in brightness upon ligand addition ($\Delta F/F_o < -5\%$), 59.6% had no fluorescence response ($-5\% < \Delta F/F_o < 5\%$), and 10.1% increase in fluorescence ($\Delta F/F_o > 5\%$). We recovered the sensor cDNA from cells with the highest response amplitude by RT-PCR and sequenced the PCR product. Sensor cDNA was cloned into mammalian expression vectors for subsequent characterization in HEK293 cultures. We called the best-performing sensor dMASS[1], indicating that the sensor has been optimized through Opto-MASS screening. All of dMASS[1]'s targeted linker sites were mutated compared to the parent dLight1.1 scaffold (Figure 3G). Next, we tested dMASS[1] in standard HEK293 cell cultures. dMASS[1] had a lower K_D than the parent construct, dLight1.1 (K_D = 323 and 625 nM, respectively, Figure 4A, and a 1.6-fold larger signal at 10 μM DA ($p < 0.0001$, Student's t test, unpaired, Figure 4B). The baseline fluorescence of dMASS[1] was not significantly different compared to that of dLight1.1 ($p = 0.0734$, unpaired Student's t test, Figure 4C). dMASS[1] and dLight1.1 also have similar ligand specificities (Figure 4D). Previous studies compared sensors using confocal microscopy, while our validations are routinely done under epifluorescence. Hence, we compared

https://doi.org/10.1021/acssensors.3c01573
ACS Sens. 2023, 8, 4233−4244

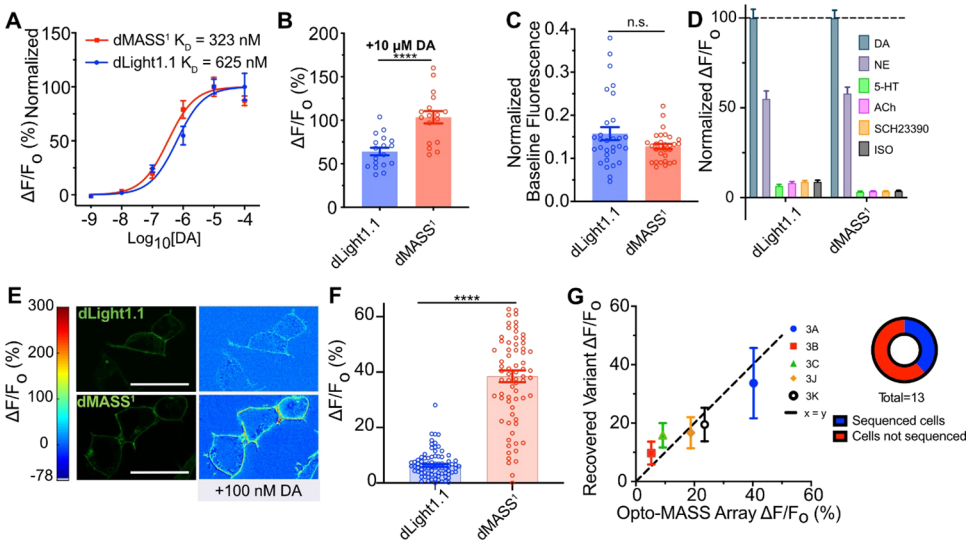

Figure 4. dMASS[1] biophysical characterization in HEK293 cells. (A) Comparison of the apparent dopamine affinity curves of the parent scaffold dLight1.1 and dMASS[1] under epifluorescence microscopy (single site binding 18 cells, unpaired *t* test). (B) dLight1.1 and dMASS[1] response to saturating 10 μM DA in HEK293 mammalian cell cultures. ($p < 0.0001$, unpaired *t* test, $n = 5-6$ cells/well, 3 wells). (C) Baseline fluorescence comparison of dLight1.1 and dMASS[1] normalized to C-terminally tagged mRuby3 (negative control). ($p = 0.0734$, unpaired Student's *t* test). (D) Pharmacological specificity of dLight1.1 and dMASS[1] to 10 μM of compounds, normalized to 10 μM DA stimulation (dLight1.1 100 ± 4.85%, dMASS[1] 100 ± 4.29), NE is norepinephrine (dLight1.1 55.06 ± 4.31 dMASS[1] 58.00 ± 3.46%), 5-HT is 5-hydroxytryptamine (dLight1.1 6.61 ± 0.69% dMASS[1] 3.32 ± 0.20%), ACh is acetylcholine (dLight1.1 8.22 ± 0.58%, dMASS[1] 3.61 ± 0.14%), SCH23390 (D_1 receptor antagonist dLight1.1 8.87 ± 0.58%, dMASS[1] 3.58 ± 0.16%), and Iso is isoproterenol (dLight1.1 8.89 ± 0.83%, dMASS[1] 3.80 ± 0.21%). $N = 40$ cells. All plots are mean ± SEM. (E) Representative confocal images of HEK293 cells expressing dopamine sensors and membrane-localized responses to 100 nM dopamine bath application. Thirty μm scale bar. (F) Average dLight1.1 and dMASS[1] membrane-localized responses in HEK293 cells to 100 nM dopamine imaged on a confocal microscope (86 and 69 cells, respectively, $p < 0.0001$, two-tailed *t* test). (G) Posthoc analysis of variants recovered from Opto-MASS PDMS arrays and compared to signal response under 500 nM dopamine in HEK cell populations ($N > 20$). Of the 13 retrieved cells, 5 yielded cDNA after single-cell RT-PCR. The average response amplitude matched the individual response measured during the Opto-MASS screen.

dMASS[1] to dLight1.1 at a lower 100 nM dopamine, using a confocal microscope to align our measurements with other publications (Figure 4E,F). Here, dMASS[1] also outperforms dLight1.1 by greater than 6-fold ($p < 0.0001$, two-tailed *t* test), demonstrating its enhanced properties under this use scenario. We retrieved the cDNA from 5 out of 13 individual cells picked from the Opto-MASS PDMS arrays, resulting in a recovery rate of 38% (Figure 4G, Table S2). Future optimization of the retrieval process will further enhance this number. A retrospective analysis of the single-cell performance on Opto-MASS arrays revealed that they closely matched the population response of the retrieved variants in HEK cells (Figure 4G).

Additionally, we compared the performance of dLight1.1, dMASS[1], and the dopamine sensor $GRAB_{DA2m}$ in HEK293 cells (Figure S2). dMASS[1] matches $GRAB_{DA2m}$ closely in dopamine and norepinephrine selectivity. However, $GRAB_{DA2m}$ provides larger response amplitudes. $GRAB_{DA2m}$ utilizes the human dopamine receptor 2 (DRD2) as the ligand binding domain, while dMASS is based on DRD1. Therefore, we tested whether both sensors have different responses toward DRD1 and DRD2 specific antagonists. Sulpiride is a specific DRD2 antagonist and inhibits DA-dependent responses from $GRAB_{DA2m}$ but not dMASS[1] (Figure S2F). In contrast, as a selective DRD1 antagonist, SCH 23390 inhibits dMASS[1] but not $GRAB_{DA2m}$. As a reported DRD2 antagonist, haloperidol not only inhibits $GRAB_{DA2m}$ responses as expected but also significantly lowers the dMASS[1] response to DA. These results suggest that selective DRD antagonists can be used in experiments in combination with dopamine sensors. However, the dopamine sensors of choice have to be insensitive to the chosen antagonists. Depending on the research objective, dMASS1 or GRABDA2m can be used with antagonists but should be selected based on their pharmacological profiles.

Opto-MASS High-Throughput Engineering of a Neuropeptide Sensor. After the initial validation of Opto-MASS, we developed a sensor for ligands for which only limited solutions currently exist. Specifically, techniques to monitor opioids either lack cell-type specificity or are incompatible with real-time imaging.[21−24] Opioid peptides help regulate motivation, stress, reward, gastrointestinal mobility, hedonic homeostasis, feeding, and other behaviors.[25−28] The different biological roles are mediated through several subtypes of opioid receptors (mu, delta, kappa, nociceptin). However, the receptor sensitivity to diverse endogenous and exogenous opioids varies, and the ligands are rarely exclusive to just one receptor.[29] The genetically encoded opioid sensor M-SPOTIT2 utilizes the mu-opioid receptor but has hour-long on-and-off kinetics and requires high pH values for activation.[22] We selected to optimize sensor prototype called mLight based on the Mu-opioid GPCR (MOR) for optimization.[4] The prototype suffered from poor dynamic range and poor cell surface expression, precluding it from *in vivo* use.[4] First, we validated that the published cpGFP domain insertion was the most optimal position (Figure S3A,B). We then enhanced membrane trafficking by adding membrane trafficking and endoplasmic reticulum export sequences (TS-ER) (Figure S3C).[30] To increase the allosteric coupling between cpGFP and MOR, we targeted four residues

https://doi.org/10.1021/acssensors.3c01573
ACS Sens. 2023, 8, 4233−4244

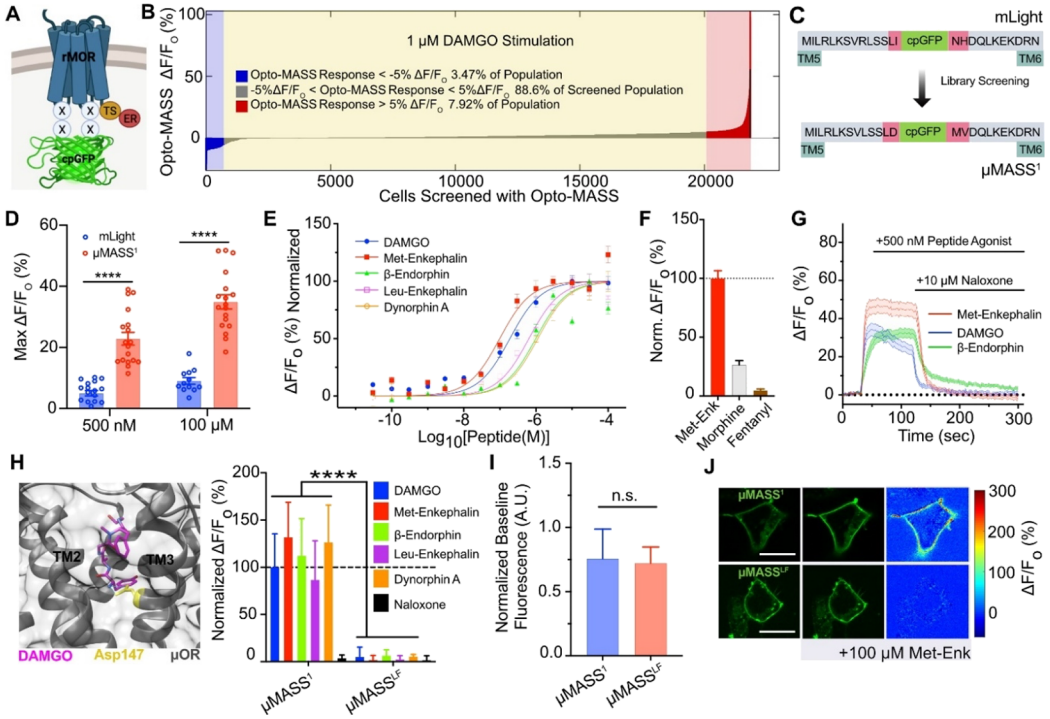

Figure 5. Engineering of the opioid sensor μMASS[1] with Opto-MASS and its *in vitro* biophysical characterization. (A) cpGFP receptor insertion into rat mu-opioid receptor (MOR) and locations of linker residues targeted by site-saturated mutation for generating a MOR sensor library. We added the membrane trafficking signals TS-ER to the c-terminus.[38] (B) Aggregated sensor library response using Opto-MASS. 21,839 cells were screened over 2 days, resulting in 3.47% with a ligand-dependent decrease in fluorescence ($\Delta F/F_o < -5\%$), 88.6% with no change in fluorescence ($-5\% < \Delta F/F_o < 5\%$), and 7.92% with an increase in fluorescence ($\Delta F/F_o > 5\%$). (C) Mutational changes in the selected variant μMASS[1] compared to those of the parent scaffold mLight. (D) mLight and μMASS[1] response to 500 nM (mLight 5.00 ± 0.87%; μMASS[1]: 22.9 ± 2.1%) and 100 μM DAMGO (mLight 9.06 ± 1.11, μMASS[1] 34.31 ± 3.11). $P < 0.0001$, unpaired t test $n = 12-18$ cells, 2–3 wells. (E) Apparent affinity curves of μMASS[1] for common opioid peptides and DAMGO. K_D as follows: DAMGO 243 nM, methionine-enkephalin 99 nM, leucine-enkephalin 637 nM, β-endorphin 1176 nM, and dynorphin A 1125 nM. $n = 18$ cells/3 wells each. (F) μMASS[1]'s normalized response to 1 μM endogenous and exogenous opioids, morphine, and fentanyl ($n = 19-21$ cells, three wells). (G) μMASS[1] responses are reversible by the addition of opioid receptor antagonist naloxone. $N = 27-28$ cells/3 wells. (H) Left: the mutated residue for generating a loss of function variant from μMASS[1] is highlighted in yellow (PDB ID: 6DDF). Right: comparison of μMASS[1] and μMASS[LF] (loss-of-function) ligand responses, which were normalized to 10 μM DAMGO (unpaired t test, **** $p < 0.0001$, $n = 3$ wells, 6–9 cells per well). (I) μMASS[1] and μMASS[LF] do not have significantly different baseline fluorescence. The fluorescence was normalized to a C terminally tagged mRuby3 ($p = 0.90$ unpaired t test with Welch's correction; $n = 16-27$ cells/2–3 wells, mean ± SEM). (J) Representative confocal images of μMASS[1] and μMASS[LF] expressed in HEK293 cells and their responses to 100 μM met-enkephalin.

within the linkers between the domains (Figure 5A). We screened >21,000 cells in two rounds of screening under 1 μM [D-Ala[2], N-MePhe[4], Gly-ol]-enkephalin (DAMGO) stimulation (Figure 5B). DAMGO is a synthetic enkephalin with high specificity for the MOR. We recovered a high-performing variant and dubbed it μMASS[1]. All targeted positions were mutated in uMASS[1] compared to those in mLight (Figure 5C). μMASS[1] had significantly better responses to nonsaturating 500 nM (~4.6 fold improved over mLight) and saturating concentrations of DAMGO (~3.8 fold improved over mLight) compared to the parent construct (Figure 5D). Similar to the native MOR, μMASS[1] could detect several types of opioid peptides, such as the Met- and Leu-enkephalins, dynorphin A and β-endorphin with differing apparent affinities (Figure 5E, DAMGO K_D = 243 nM, methionine-enkephalin K_D = 99 nM, leucine-enkephalin K_D = 637 nM, β-endorphin K_D = 1176 nM, dynorphin A K_D = 1125 nM[29]). The exogenous MOR agonists morphine and fentanyl (at 1 μM) activated μMASS[1] at lower levels compared to Met-enk (26.4 ± 3.64 and 4.63 ± 1.23%, respectively) (Figure 5F). We demonstrated that the sensor activity is reversible by applying the opioid receptor antagonist naloxone, which abolished the fluorescence signal and could be used as an *in vivo* pharmacological control (Figure 5G). Also, we engineered a loss of function (LF) variant, μMASS[LF], by mutating Asp147[3.32]Gly (Ballesteros Weinstein numbering[31]). Asp147[3.32] is hypothesized to coordinate a critical intermolecular bond with the primary amine in the canonical opioid signaling motif.[32−35] The μMASS[LF] response signal to 10 μM various opioid peptides was abolished (Figure 5H). At the same time, it had a similar baseline fluorescence compared to that of the parent μMASS[1] (Figure 5I $p = 0.90$, unpaired t test, Welch's correction). Additionally, μMASS[LF] lacks any membrane-localized fluorescence changes when imaged under confocal microscopy (Figure 5J). Also, μMASS[1] did not have any significant ligand-dependent internalization in HEK293 cells when exposed to 10 μM DAMGO and imaged over an hour at 37 °C in comparison to a C-terminally tagged rat MOR (Figure S3D−F).

Our innovative functional analysis of sensor libraries in mammalian host cells is a long-sought goal in sensor engineering. We can test signal amplitudes of thousands of variants under physiological conditions in minutes and, thus, rapidly identify high-performance sensor variants. In essence, Opto-MASS emulates high-throughput screening methods

https://doi.org/10.1021/acssensors.3c01573
ACS Sens. 2023, 8, 4233−4244

using bacteria or yeast. However, these methods present potential problems when expressing mammalian proteins, such as membrane-bound GPCRs. Opto-MASS circumvents difficulties in protein folding, stability, and membrane trafficking by harnessing a mammalian expression system. Furthermore, Opto-MASS directly links phenotype and genotype of variants while the throughput or variant numbers are higher than comparable sensor screening platforms in mammalian cells[14−18] (Table 1). As demonstrated, we tested ∼13,000 dopamine and ∼21,000 mu-opioid sensor variants and identified dMASS[1] and μMASS[1] within 1 month after library generation. Users implementing Opto-MASS will need to balance the library size, desired screening outcomes, and resources when choosing their approach. For example, we used NNK codons to introduce variability with a reduction in nonsense mutations (from three to one codon) while retaining all 20 amino acids. However, with this mutational scheme, approximately 12% of our library contains a stop codon and is not expressed in mammalian cells. Future users could implement other mutational schemes, such as NDT codons, for smaller library sizes and target fewer locations to increase the statistical coverage of sensor libraries during screening. While NDT codons are restricted to 12 amino acids, they include all the main biophysical properties of the 20 essential amino acids.[36] Importantly, Opto-MASS has the potential for improvement in future iterations. First, the Opto-MASS's cDNA recovery rate is currently around 30−40%. Increasing the retrieval of genetic information by optimizing cell aspiration and single-cell RT-PCR is a critical future goal that could further maximize efficiency. The efficiency could be enhanced even more by including FACS prescreens. Most sensor variants did not visibly respond to ligand applications, i.e. they were loss-of-function mutations or generated less desirable negative signal amplitudes. Hence, removing dim cells under ligand exposure would effectively reduce the number of cells that must be tested by Opto-MASS.

We expect that dMASS[1] would be compatible with *in vivo* applications, as its parent construct dLight1.1, has been widely adopted for experiments in rodent brains.[4] The enhanced dynamic range may improve sensor performance over dLight1.1 while providing a different pharmacological profile than $GRAB_{DA2m}$ (Figure S2). However, many aspects must be considered for *in vivo* experiments. The performance of most sensors is influenced by factors such as the efficiency of the viral delivery, expression profile (e.g., presynaptic vs postsynaptic, dense vs sparse sensor expression), targeted cell types, and background fluorescence of tissue. Furthermore, the basal ligand concentration could differ between brain regions, resulting in differences in the sensor's baseline fluorescence and response amplitudes. Specifically, endogenous peptide release can confound *in vivo* performance, as neuropeptides, such as opioids, are hypothesized to be released at lower concentrations and diffuse over longer distances than classical neurotransmitters. The lack of precise real-time methods to detect endogenous opioid release led to a lack of understanding of these processes' spatial and temporal dynamics. Thus, detecting endogenous opioids using μMASS[1] or other opioid sensors will first require testing under evoked release paradigms, such as optogenetic or chemogenetic stimulation of enkephalin release from PENK-positive neurons or endorphins from POMC neurons. This could be followed by natural behaviors such as reward stimuli measured in regions known to express mu-opioid receptors or release opioids, such as the periaqueductal gray, nucleus accumbens shell, or ventral tegmental area. The variety of endogenous opioids and their different physiological functions in various brain regions could necessitate the development of opioid sensors with specific ligand binding profiles (e.g., enkephalin vs endorphin), kinetics, and ligand affinities to match the physiological parameters of the expected opioid release. The fast optimization of dMASS[1] and μMASS[1], positions Opto-MASS and other high-throughput approaches[14−18] as ideal facilitators of further sensor development.

Opto-MASS is a pioneering approach in GEFI engineering suited to develop GEFIs for approximately 800 GPCRs in the human genome. Using trial-and-error mutagenesis would make this an otherwise resource- and time-intensive task. Opto-MASS requires only one step for library generation, host cell transfection, selection, and cell expansion. Tens of thousands of variants can be tested within one month after conceptualizing a sensor engineering strategy. Therefore, the broad adaptation of Opto-MASS could significantly accelerate the development of high-performance sensors for a wide range of biomedical applications.

Materials. The following plasmid vectors are available from Addgene.org: pAAV_hsyn_HA-Flag-uMASS_1_WPRE (#209760), pAAV_hsyn_HA_Flag-uMASS_LF (#209761), p3.1CAG-uMASS_1 (#209762), p3.1CAG_uMASS_LF (#209763), p3.1CMV_dMASS_1 (#209764), pAAV_hsyn-dMASS_1_WPRE (#209765), pAAV_hsyn-dMASS_LF_WPRE (#209766).

■ ASSOCIATED CONTENT

Supporting Information

The Supporting Information is available free of charge at https://pubs.acs.org/doi/10.1021/acssensors.3c01573.

Use of control fluorophore during screening; DA sensor in vitro biophysical characterization and comparison; design, engineering, and characterization of μMASS libraries and extended biophysical characterization of optimized variants; data summary of dopamine sensor library recovery; genetic and protein sequences of indicators developed; and primers used in this study (PDF)

■ AUTHOR INFORMATION

Corresponding Author

Andre Berndt − *Department of Bioengineering, University of Washington, Seattle, Washington 98105, United States; Institute of Stem Cell and Regenerative Medicine, University of Washington, Seattle, Washington 98109, United States;* orcid.org/0000-0003-4758-5598; Email: berndtuw@uw.edu

Authors

Michael Rappleye − *Department of Bioengineering, University of Washington, Seattle, Washington 98105, United States; Institute of Stem Cell and Regenerative Medicine, University of Washington, Seattle, Washington 98109, United States;* Present Address: Now at: Institute of Pharmacology and Toxicology, University of Zurich, Winterthurerstrasse 190, 8057 Zürich, Switzerland (M.R.); orcid.org/0000-0002-2885-3406

Sarah J. Wait − *Institute of Stem Cell and Regenerative Medicine, University of Washington, Seattle, Washington*

https://doi.org/10.1021/acssensors.3c01573
ACS Sens. 2023, 8, 4233−4244

98109, United States; Molecular Engineering and Sciences Institute, University of Washington, Seattle, Washington 98195, United States; orcid.org/0000-0001-5660-2391

Justin Daho Lee − *Institute of Stem Cell and Regenerative Medicine, University of Washington, Seattle, Washington 98109, United States; Molecular Engineering and Sciences Institute, University of Washington, Seattle, Washington 98195, United States;* orcid.org/0000-0002-0284-2389

Jamison C. Siebart − *The Wallace H. Coulter Department of Biomedical Engineering, Georgia Institute of Technology, Atlanta, Georgia 30332, United States;* orcid.org/0000-0002-0424-7487

Lily Torp − *Department of Bioengineering, University of Washington, Seattle, Washington 98105, United States; Institute of Stem Cell and Regenerative Medicine, University of Washington, Seattle, Washington 98109, United States*

Netta Smith − *Department of Bioengineering, University of Washington, Seattle, Washington 98105, United States; Institute of Stem Cell and Regenerative Medicine, University of Washington, Seattle, Washington 98109, United States*

Jeanot Muster − *Department of Bioengineering, University of Washington, Seattle, Washington 98105, United States; Institute of Stem Cell and Regenerative Medicine, University of Washington, Seattle, Washington 98109, United States;* orcid.org/0000-0002-1972-6851

Kenneth A. Matreyek − *Department of Pathology, Case Western Reserve University School of Medicine, Cleveland, Ohio 44106, United States;* orcid.org/0000-0001-9149-551X

Douglas M. Fowler − *Department of Genome Sciences, Seattle, Washington 98195-5065, United States;* orcid.org/0000-0001-7614-1713

Complete contact information is available at: https://pubs.acs.org/10.1021/acssensors.3c01573

Notes

The authors declare no competing financial interest.

■ ACKNOWLEDGMENTS

A.B. was supported by The Brain Research Foundation, UW Royalty Research Fund, UW ISCRM IPA, NIGMS R01 GM139850-01, P30 DA048736-01-Pilot, NIMH RF1MH130391, NINDS U01NS128537, NIDA R21DA051193 and the McKnight Foundation's Technologies in Neuroscience Award. K.A.M. was supported by NIGMS R35 GM142886, D.M.F. was supported by NHGRI RM1 HG010461, and NIGMS R01 GM109110. D.C.C. was supported by K99DA049862, and R00DA049862. S.J.W. was supported by DGE-2140004. The research received additional support from the Lynn and Mike Garvey Imaging Core, the UW NAPE Center, and ISCRM Shared Equipment. We want to thank Dr. Randy Moon for his support. Part of this work was conducted at the Washington Nanofabrication Facility/Molecular Analysis Facility, a National Nanotechnology Coordinated Infrastructure (NNCI) site at the University of Washington with partial support from the National Science Foundation via awards NNCI-1542101 and NNCI-2025489. Some figures were created with Biorender.com[38] and ChimeraX (http://www.cgl.ucsf.edu/chimera).[39]

■ REFERENCES

(1) Baird, G. S.; Zacharias, D. A.; Tsien, R. Y. Circular permutation and receptor insertion within green fluorescent proteins. *Proc. Natl. Acad. Sci. U.S.A.* **1999**, *96* (20), 11241−11246.

(2) Chen, T. W.; Wardill, T. J.; Sun, Y.; Pulver, S. R.; Renninger, S. L.; Baohan, A.; Schreiter, E. R.; Kerr, R. A.; Orger, M. B.; Jayaraman, V.; Looger, L. L.; Svoboda, K.; Kim, D. S. Ultrasensitive fluorescent proteins for imaging neuronal activity. *Nature* **2013**, *499* (7458), 295−300.

(3) Villette, V.; Chavarha, M.; Dimov, I. K.; Bradley, J.; Pradhan, L.; Mathieu, B.; Evans, S. W.; Chamberland, S.; Shi, D.; Yang, R.; Kim, B. B.; Ayon, A.; Jalil, A.; St-Pierre, F.; Schnitzer, M. J.; Bi, G.; Toth, K.; Ding, J.; Dieudonné, S.; Lin, M. Z. Ultrafast Two-Photon Imaging of a High-Gain Voltage Indicator in Awake Behaving Mice. *Cell* **2019**, *179* (7), 1590−1608.e23.

(4) Patriarchi, T.; Cho, J. R.; Merten, K.; Howe, M. W.; Marley, A.; Xiong, W. H.; Folk, R. W.; Broussard, G. J.; Liang, R.; Jang, M. J.; Zhong, H.; Dombeck, D.; von Zastrow, M.; Nimmerjahn, A.; Gradinaru, V.; Williams, J. T.; Tian, L. Ultrafast neuronal imaging of dopamine dynamics with designed genetically encoded sensors. *Science* **2018**, *360* (6396), No. eaat4422.

(5) Sun, F.; Zeng, J.; Jing, M.; Zhou, J.; Feng, J.; Owen, S. F.; Luo, Y.; Li, F.; Wang, H.; Yamaguchi, T.; Yong, Z.; Gao, Y.; Peng, W.; Wang, L.; Zhang, S.; Du, J.; Lin, D.; Xu, M.; Kreitzer, A. C.; Cui, G.; Li, Y. A Genetically Encoded Fluorescent Sensor Enables Rapid and Specific Detection of Dopamine in Flies, Fish, and Mice. *Cell* **2018**, *174* (2), 481−496.e19.

(6) Rosenbaum, D. M.; Rasmussen, S. G.; Kobilka, B. K. The structure and function of G-protein-coupled receptors. *Nature* **2009**, *459* (7245), 356−363.

(7) Feng, J.; Zhang, C.; Lischinsky, J. E.; Jing, M.; Zhou, J.; Wang, H.; Zhang, Y.; Dong, A.; Wu, Z.; Wu, H.; Chen, W.; Zhang, P.; Zou, J.; Hires, S. A.; Zhu, J. J.; Cui, G.; Lin, D.; Du, J.; Li, Y. A Genetically Encoded Fluorescent Sensor for Rapid and Specific In Vivo Detection of Norepinephrine. *Neuron* **2019**, *102* (4), 745−761.e8.

(8) Dong, C.; Ly, C.; Dunlap, L. E.; Vargas, M. V.; Sun, J.; Hwang, I. W.; Azinfar, A.; Oh, W. C.; Wetsel, W. C.; Olson, D. E.; Tian, L. Psychedelic-inspired drug discovery using an engineered biosensor. *Cell* **2021**, *184* (10), 2779−2792.e18.

(9) Duffet, L.; Kosar, S.; Panniello, M.; Viberti, B.; Bracey, E.; Zych, A. D.; Radoux-Mergault, A.; Zhou, X.; Dernic, J.; Ravotto, L.; Tsai, Y. C.; Figueiredo, M.; Tyagarajan, S. K.; Weber, B.; Stoeber, M.; Gogolla, N.; Schmidt, M. H.; Adamantidis, A. R.; Fellin, T.; Burdakov, D.; Patriarchi, T. A genetically encoded sensor for in vivo imaging of orexin neuropeptides. *Nat. Methods* **2022**, *19* (2), 231−241.

(10) Li, Y.; Jing, M.; Zhang, P.; Wang, G.; Feng, J.; Mesik, L.; Zeng, J.; Jiang, H.; Wang, S.; Looby, J. C.; Guagliardo, N. A.; Langma, L. W.; Lu, J.; Zuo, Y.; Talmage, D. A.; Role, L. W.; Barrett, P. Q.; Zhang, L. I.; Luo, M.; Song, Y.; Zhu, J. J. A genetically encoded fluorescent acetylcholine indicator for in vitro and in vivo studies. *Nat. Biotechnol.* **2018**, *201836* (8), 726 DOI: 10.1038/nbt.4184.

(11) Tian, L.; Hires, S. A.; Mao, T.; Huber, D.; Chiappe, M. E.; Chalasani, S. H.; Petreanu, L.; Akerboom, J.; McKinney, S. A.; Schreiter, E. R.; Bargmann, C. I.; Jayaraman, V.; Svoboda, K.; Looger, L. L. Imaging neural activity in worms, flies and mice with improved GCaMP calcium indicators. *Nat. Methods* **2009**, *6* (12), 875−881.

(12) Hackley, C. R.; Mazzoni, E. O.; Blau, J. cAMPr: A single-wavelength fluorescent sensor for cyclic AMP. *Science signaling* **2018**, *11* (520), No. eaah3738.

(13) Hauser, A. S.; Attwood, M. M.; Rask-Andersen, M.; Schiöth, H. B.; Gloriam, D. E. Trends in GPCR drug discovery: new agents, targets and indications. *Nature reviews. Drug discovery* **2017**, *16* (12), 829−842.

(14) Wardill, T. J.; Chen, T. W.; Schreiter, E. R.; Hasseman, J. P.; Tsegaye, G.; Fosque, B. F.; Behnam, R.; Shields, B. C.; Ramirez, M.; Kimmel, B. E.; Kerr, R. A.; Jayaraman, V.; Looger, L. L.; Svoboda, K.; Kim, D. S. A neuron-based screening platform for optimizing genetically-encoded calcium indicators. *PloS one* **2013**, *8* (10), No. e77728.

(15) Piatkevich, K. D.; Jung, E. E.; Straub, C.; Linghu, C.; Park, D.; Suk, H. J.; Hochbaum, D. R.; Goodwin, D.; Pnevmatikakis, E.; Pak, N.; Kawashima, T.; Yang, C. T.; Rhoades, J. L.; Shemesh, O.; Asano, S.; Yoon, Y. G.; Freifeld, L.; Saulnier, J. L.; Riegler, C.; Engert, F.; Hughes, T.; Drobizhev, M.; Szabo, B.; Ahrens, M. B.; Flavell, S. W.; Sabatini, B. L.; Boyden, E. S. A robotic multidimensional directed evolution approach applied to fluorescent voltage reporters. *Nat Chem Biol* **2018**, *14* (4), 352−360.
(16) Koveal, D.; Rosen, P. C.; Meyer, D. J.; Díaz-García, C. M.; Wang, Y.; Cai, L. H.; Chou, P. J.; Weitz, D. A.; Yellen, G. A high-throughput multiparameter screen for accelerated development and optimization of soluble genetically encoded fluorescent biosensors. *Nat. Commun* **2022**, *13* (1), 2919.
(17) Lin, C.; Liu, L.; Zou, P. Functional imaging-guided cell selection for evolving genetically encoded fluorescent indicators. *Cell reports methods* **2023**, *3* (8), No. 100544.
(18) Erdogan, M.; Fabritius, A.; Basquin, J.; Griesbeck, O. Targeted In Situ Protein Diversification and Intra-organelle Validation in Mammalian Cells. *Cell Chem. Biol.* **2020**, *27* (5), 610−621.e5.
(19) Matreyek, K. A.; Stephany, J. J.; Fowler, D. M. A platform for functional assessment of large variant libraries in mammalian cells. *Nucleic acids research* **2017**, *45* (11), No. e102.
(20) Nasu, Y.; Shen, Y.; Kramer, L.; Campbell, R. E. Structure- and mechanism-guided design of single fluorescent protein-based biosensors. *Nat. Chem. Biol.* **2021**, *17* (5), 509−518.
(21) Al-Hasani, R.; Wong, J. T.; Mabrouk, O. S.; McCall, J. G.; Schmitz, G. P.; Porter-Stransky, K. A.; Aragona, B. J.; Kennedy, R. T.; Bruchas, M. R. In vivo detection of optically-evoked opioid peptide release. *eLife* **2018**, *7*, No. e36520.
(22) Kroning, K. E.; Li, M.; Petrescu, D. I.; Wang, W. A genetically encoded sensor with improved fluorescence intensity for opioid detection at cellular resolution. *Chemical communications (Cambridge, England)* **2021**, *57* (81), 10560−10563.
(23) Stoeber, M.; Jullié, D.; Lobingier, B. T.; Laeremans, T.; Steyaert, J.; Schiller, P. W.; Manglik, A.; von Zastrow, M. A Genetically Encoded Biosensor Reveals Location Bias of Opioid Drug Action. *Neuron* **2018**, *98* (5), 963−976.e5.
(24) Kroning, K. E.; Wang, W. Designing a Single Protein-Chain Reporter for Opioid Detection at Cellular Resolution. *Angewandte Chemie (International ed. in English)* **2021**, *60* (24), 13358−13365.
(25) Castro, D. C.; Oswell, C. S.; Zhang, E. T.; Pedersen, C. E.; Piantadosi, S. C.; Rossi, M. A.; Hunker, A. C.; Guglin, A.; Morón, J. A.; Zweifel, L. S.; Stuber, G. D.; Bruchas, M. R. An endogenous opioid circuit determines state-dependent reward consumption. *Nature* **2021**, *598* (7882), 646−651.
(26) Shippenberg, T. S.; Herz, A. Differential effects of mu and kappa opioid systems on motivational processes. *NIDA Res. Monograph* **1986**, *75*, 563−566.
(27) Land, B. B.; Bruchas, M. R.; Lemos, J. C.; Xu, M.; Melief, E. J.; Chavkin, C. The dysphoric component of stress is encoded by activation of the dynorphin kappa-opioid system. *J. Neurosci.* **2008**, *28* (2), 407−414.
(28) Matthes, H. W.; Maldonado, R.; Simonin, F.; Valverde, O.; Slowe, S.; Kitchen, I.; Befort, K.; Dierich, A.; Le Meur, M.; Dollé, P.; Tzavara, E.; Hanoune, J.; Roques, B. P.; Kieffer, B. L. Loss of morphine-induced analgesia, reward effect and withdrawal symptoms in mice lacking the mu-opioid-receptor gene. *Nature* **1996**, *383* (6603), 819−823.
(29) Fricker, L. D.; Margolis, E. B.; Gomes, I.; Devi, L. A. Five Decades of Research on Opioid Peptides: Current Knowledge and Unanswered Questions. *Molecular pharmacology* **2020**, *98* (2), 96−108.
(30) Gradinaru, V.; Zhang, F.; Ramakrishnan, C.; Mattis, J.; Prakash, R.; Diester, I.; Goshen, I.; Thompson, K. R.; Deisseroth, K. Molecular and cellular approaches for diversifying and extending optogenetics. *Cell* **2010**, *141* (1), 154−165.
(31) Ballesteros, J. A.; Weinstein, H. Integrated methods for the construction of three-dimensional models and computational probing of structure-function relations in G protein-coupled receptors. *Methods in Neurosciences* **1995**, *25*, 366−428.
(32) Manglik, A.; Kruse, A. C.; Kobilka, T. S.; Thian, F. S.; Mathiesen, J. M.; Sunahara, R. K.; Pardo, L.; Weis, W. I.; Kobilka, B. K.; Granier, S. Crystal structure of the μ-opioid receptor bound to a morphinan antagonist. *Nature* **2012**, *485* (7398), 321−326.
(33) Granier, S.; Manglik, A.; Kruse, A. C.; Kobilka, T. S.; Thian, F. S.; Weis, W. I.; Kobilka, B. K. Structure of the δ-opioid receptor bound to naltrindole. *Nature* **2012**, *485* (7398), 400−404.
(34) Koehl, A.; Hu, H.; Maeda, S.; Zhang, Y.; Qu, Q.; Paggi, J. M.; Latorraca, N. R.; Hilger, D.; Dawson, R.; Matile, H.; Schertler, G. F. X.; Granier, S.; Weis, W. I.; Dror, R. O.; Manglik, A.; Skiniotis, G.; Kobilka, B. K. Structure of the μ-opioid receptor-Gi protein complex. *Nature* **2018**, *558* (7711), 547−552.
(35) Huang, W.; Manglik, A.; Venkatakrishnan, A. J.; Laeremans, T.; Feinberg, E. N.; Sanborn, A. L.; Kato, H. E.; Livingston, K. E.; Thorsen, T. S.; Kling, R. C.; Granier, S.; Gmeiner, P.; Husbands, S. M.; Traynor, J. R.; Weis, W. I.; Steyaert, J.; Dror, R. O.; Kobilka, B. K. Structural insights into μ-opioid receptor activation. *Nature* **2015**, *524* (7565), 315−321.
(36) Reetz, M. T.; Kahakeaw, D.; Lohmer, R. Addressing the numbers problem in directed evolution. *Chembiochem: a European journal of chemical biology* **2008**, *9* (11), 1797−1804.
(37) Dana, H.; Sun, Y.; Mohar, B.; Hulse, B. K.; Kerlin, A. M.; Hasseman, J. P.; Tsegaye, G.; Tsang, A.; Wong, A.; Patel, R.; Macklin, J. J.; Chen, Y.; Konnerth, A.; Jayaraman, V.; Looger, L. L.; Schreiter, E. R.; Svoboda, K.; Kim, D. S. High-performance calcium sensors for imaging activity in neuronal populations and microcompartments. *Nat. Methods* **2019**, *16* (7), 649−657.
(38) Images were created using BioRender.com.
(39) Pettersen, E. F.; Goddard, T. D.; Huang, C. C.; Couch, G. S.; Greenblatt, D. M.; Meng, E. C.; Ferrin, T. E. UCSF Chimera–a visualization system for exploratory research and analysis. *Journal of computational chemistry* **2004**, *25* (13), 1605−1612.

https://doi.org/10.1021/acssensors.3c01573
ACS Sens. 2023, 8, 4233−4244